Nanoscale Advances

PAPER

View Article Online
View Journal | View Issue

Cite this: *Nanoscale Adv.*, 2019, **1**, 627

Synthesis and characterization of silver nanoparticle-loaded amorphous calcium phosphate microspheres for dental applications†

Mayuresh Keskar, [a] Camila Sabatini, [b] Chong Cheng [a] and Mark T. Swihart *[a]

The goals of this work were (1) to synthesize composite nanostructures comprised of amorphous calcium phosphate (ACP) loaded with silver nanoparticles using a spray pyrolysis method and (2) to demonstrate their potential for use in dental adhesives. Release of silver ions from these nanostructures could provide antibacterial activity, while release of calcium and phosphate ions could promote tooth remineralization. Precursor solutions were prepared with varying silver concentrations corresponding to 5, 10, and 15 mol% of the calcium content, then sprayed into a furnace (550 °C) as droplets with a mean diameter near 2 μm. In this process, each droplet is converted into a single solid microsphere *via* rapid heating. The synthesized particles were collected using a polymeric filter installed at the end of the reaction zone. Different quantities (2, 5, and 10 wt%) of the nanocomposite material were mixed with a commercially available dental adhesive (Single Bond, 3M ESPE) which was then polymerized into discs for incubation in a solution simulating cariogenic conditions. Release of silver, calcium and phosphorus ions into the solution was measured for 1 month. The nanostructures of ~10 nm silver nanoparticles embedded into 100 nm to 2 μm ACP particles demonstrated good dispersion in the adhesive resin blend, which in application would shield surrounding tissues from direct contact with silver. The composite nanoparticles provided a quick initial release of ions after which the concentration of calcium, phosphorous, and silver in the incubation solution remained constant or increased slightly. The dispersibility and ion release of the new nanostructures may offer potential for use in dental materials to achieve anti-bacterial and remineralization effects.

Received 11th October 2018
Accepted 12th October 2018

DOI: 10.1039/c8na00281a

rsc.li/nanoscale-advances

1. Introduction

Dental caries, the most pervasive oral disease, results from tooth exposure to acid produced by bacteria that are useful in fermentation of dietary carbohydrates.[1,2] In particular, secondary caries (caries occurring at the margin or directly adjacent to a pre-existing restoration) remains the primary cause of failure for 50–70% of replacement restorations.[3] The cost of treating secondary caries in the United States alone is approximately $46 billion annually.[3] Secondary caries develops as a result of both residual bacteria after the tooth has been restored, and restoration microleakage, which provides an open pathway for bacteria to penetrate through the interface.[3]

To overcome this issue, researchers have made improvements to current dental restorative materials including resin composites and the adhesives that bind the composites to the tooth structure. Hannig *et al.* in 2010 provided a thorough review on the various nanomaterials available in preventive dentistry.[4] Modifications of the adhesive formulation, including a combination of poly(amidoamine) dendrimer (PAMAM) and dimethylaminododecyl methacrylate (DMADDM) to create anti-caries adhesives, have been studied.[5] Efforts have also been made to provide amorphous calcium phosphate (ACP) nano-precursor particles to backfill the demineralized dentin collagen by a process known as biomineralization.[1,6] Dey *et al.* have demonstrated the role of pre-nucleation clusters as building blocks for ACP, leading to formation of apatite crystals, using Cryo-TEM imaging and computer-aided three dimensional visualization.[7] Several research groups have incorporated ACP nanoparticles (NACP) into dental adhesives in an attempt to promote remineralization.[3,8–11] Xu *et al.* investigated the use of NACP in a nanocomposite, for the first time evaluating both effects of pH and NACP filler levels on ion release rate, as well as the mechanical properties of the nanocomposite.[8] Zhang *et al.* worked on the rechargeable properties of such NACP-containing composites.[12] Research efforts have concentrated on ways to provide both anti-bacterial and remineralization properties to dental materials with several agents studied by different groups.[2,13] Among these, silver has been extensively

[a]*Department of Chemical and Biological Engineering, University at Buffalo, The State University of New York, Buffalo, NY 14260, USA. E-mail: swihart@buffalo.edu*

[b]*Department of Restorative Dentistry, University at Buffalo, The State University of New York, Buffalo, NY 14260, USA*

† Electronic supplementary information (ESI) available. See DOI: 10.1039/c8na00281a

investigated due to its superior anti-bacterial efficacy compared to other materials such as zinc oxide nanoparticles and quaternary ammonium polyethylenimine nanoparticles.[2,14,15] Melo *et al.* incorporated silver and NACP as separate nanoparticles into a dental adhesive formulation with varying mass fractions of fillers. Their study, however, did not report release of calcium, phosphate and silver ions, but focused only on the evaluation of the compound's antibacterial efficacy.[10] This, unfortunately, limits the ability to make direct correlations with the presence of ions that are presumed to be responsible for the observed results. There have been previous efforts to synthesize silver-doped calcium phosphate particles,[16,17] but to the best of our knowledge, no work has demonstrated the doping/embedding of silver in amorphous calcium phosphate. ACP nucleation clusters have been identified as building blocks for crystalline apatite, and these clusters have the advantage of being more soluble under acidic conditions (which occur during caries) than crystalline forms of calcium phosphate.[18,19] Peetsch *et al.* synthesized silver-doped calcium phosphate and studied the cytotoxicity of the particles, which was an important advance in this direction. Their materials had a modest loading of silver (0.39 wt%), but when used alone, without embedding in a resin or composite, produced silver concentrations in the lethal range for human cells.[20] This leads us to explore nanostructures with higher silver loading, but potentially slower release, by incorporating silver as embedded nanoparticles within ACP, in an effort to achieve slower, sustained release of silver ions.

In this work, silver nanoparticle-loaded amorphous calcium phosphate microspheres for dental applications were synthesized and characterized. Specific objectives included producing a morphology of particles that will provide sustained release of silver ions and disperse appropriately in a dental adhesive resin formulation. Release of calcium, phosphate and silver ions from discs of adhesive resin containing the silver nanoparticle-loaded amorphous calcium phosphate microspheres under simulated cariogenic conditions was monitored over a period of 1 month.

2. Experimental

2.1. Synthesis of NACP particles

Silver–ACP nanoparticles were synthesized using a spray pyrolysis approach. The reactor system used for this is shown schematically in Fig. 1. The precursor solution consisted of calcium nitrate tetrahydrate (99+%, ACS reagent, Acros Organics), silver nitrate (0.1 N, Ricca Chemical) and *o*-phosphoric acid (85% Certified ACS, Fisher Chemical) dissolved in 80 mL DI water to give final concentrations of 150 mM calcium nitrate tetrahydrate; 100 mM *o*-phosphoric acid and 7.5 mM silver nitrate (for synthesis of particles with 5 mole percent silver relative to Ca; silver nitrate content was adjusted to achieve other silver concentrations). The calcium to phosphate molar ratio of 1.5 was maintained in each case, which is typical for synthesis of amorphous calcium phosphate particles.

The precursor solution was sprayed into the heated tube using a three-jet pressure driven atomizer (Collison type, BGI, Waltham, MA), which produced a broad size distribution of droplets ranging from <100 nm to >3 μm.[21] The droplets were carried from the atomization chamber to the furnace by an inert carrier gas flow (nitrogen, ultra-high purity, 99.999%), which was also used as a quench gas to cool the exit stream from the furnace. The gas flows were controlled using rotameters. The flow to the atomizer was controlled using nitrogen gas pressure applied to it and the fixed resistance of the jets. The reaction took place in a tubular reactor of one-inch outer diameter (Inconel tubing) with a heated length of approximately 76 cm. The furnace set point temperature was kept at 550 °C. However, the centerline temperature inside the tube may not reach the set point temperature because of the finite rate of heat transfer from the wall through the flowing gas, combined with the relatively short residence time of the gas in the reactor (~1 s).[21] The inlet pressure to the atomizer was controlled at 23–25 psig, with an additional dilution gas flow rate through the tube set at 3 lpm. The total flow entering the reactor was approximately 10 lpm. The particles were collected using a polytetrafluoroethylene (PTFE) membrane filter (pore size 0.22 μm, Tisch Scientific) attached at the end of the reaction zone. The pressure in the reaction zone was controlled using a needle valve downstream of the filter. The system was exhausted, *via* a vacuum pump, to the building chemical exhaust (fume hood) system.

2.2. Characterization of silver–ACP particles

Collected particles were stored in a freezer until ready for use to prevent crystallization of ACP. The silver–ACP nanocomposite particles were imaged using transmission electron microscopy (TEM, JEOL JEM 2010). Selected area electron diffraction (SAED) was also performed in the TEM. To prepare samples for TEM imaging, the particles were dispersed in an ethanol–water mixture and sonicated to obtain a uniform suspension which was then dropped onto a TEM grid (200 mesh copper with a carbon support film). Surface structure and elemental composition of particles were studied by scanning electron microscopy (SEM) and energy dispersive X-ray spectroscopy (EDS) using an Auriga SEM from Carl Zeiss SMT with an Oxford Instruments X-Max 20 mm^2 EDS detector. X-ray diffraction (XRD) was performed on a Rigaku Ultima IV diffractometer with a sampling width of 0.05 degree, using graphite-monochromated Cu Kα (1.54 Å) radiation at 40 kV accelerating voltage and 44 mA current. Fourier Transform Infra-Red Spectroscopy (FTIR) was performed using a Bruker Vertex 70 spectrometer, to obtain information on the surface functional groups on the particles as well as the types of bonds present in them. Thermogravimetric analysis (TGA, SDT Q-600 from TA instruments) was carried out to determine mass change of the material with changing temperature. Alumina sample pans of 90 μL volume were used for this analysis. An Inductively Coupled Plasma Optical Emission Spectrometer (ICP-OES, Thermo Scientific iCAP 6300 with iTEVA control software and UHP Ar gas for RF plasma generation) was used for measurements of the release of calcium, phosphorus, and silver ions from adhesive discs incubated in simulated cariogenic conditions.

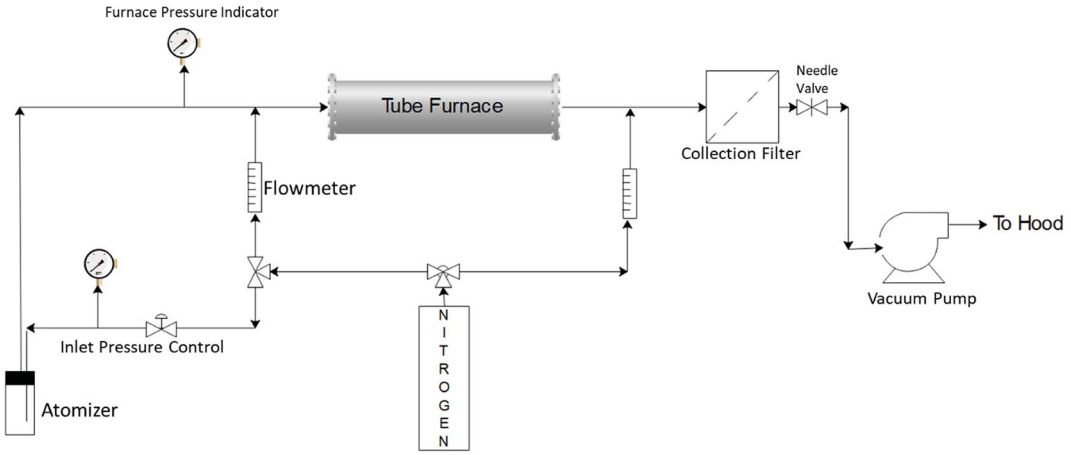

Fig. 1 Schematic of spray pyrolysis reactor setup. Precursor droplets are carried from the atomizer to the tube furnace, where the solvent evaporates and the calcium and phosphate ions react to form ACP with embedded silver nanoparticles. Particles are collected using a membrane filter.

2.3. Ion release study

To study release of silver, calcium, and phosphate ions from the nanocomposite material, the silver-embedded ACP powders were each mixed with a commercially available dental adhesive (Single Bond, 3M ESPE) in different weight percentages, and disc specimens of cured adhesive were fabricated. A total of six discs were made for each of the filler (nanocomposite particle) weight percentages in the resin and each of the molar percentages of Ag in the filler. The discs were made by polymerizing the corresponding adhesive mixture in a white PTFE mold (5 mm diameter $\times$ 1 mm high) against two glass microscope slides using a high-intensity light-emitting diode curing unit (VALO, Ultradent, South Jordan, UT, USA) with a power density of 1400 mW cm^{-2} with 20 s exposure for each disc. Glass slides were used to provide flat specimens with a uniform surface that would be less likely to introduce variations in the ion release measurements. Each set of six discs was then incubated in 100 mL of a simulated cariogenic solution containing 133 mM NaCl, which was buffered to pH 4 using a 50 mM lactic acid solution.[3] For each release measurement, 5–6 mL of the solution was pipetted out from the flasks and replaced with a fresh 133 mM NaCl solution of the same volume. The pH was then adjusted back to a value of 4 $\pm$ 0.1. The released concentrations of calcium, phosphorus, and silver ions were measured using ICP-OES at discrete time points over a period of 1 month.

3. Results and discussion

3.1. Synthesis and material characterization

Fig. 2 schematically illustrates the process of nanocomposite particle formation. Each droplet entering the spray pyrolysis reactor is converted into a single solid nanocomposite particle *via* solvent evaporation and precipitation of ACP and metallic silver. For the concentrations used here, this produces ACP particles with smaller silver nanoparticles embedded within them and/or on their surface. In the air-free environment of the spray pyrolysis reactor, silver ions are thermally reduced to zerovalent (metallic) silver at the reactor temperatures used here. The presence of silver primarily in metallic, rather than ionic, form in the product particles is expected to provide slow release of silver, due to the relatively high chemical stability of metallic silver. The relative quantity of internal *vs.* surface silver nanoparticles varies with silver concentration as discussed further below.

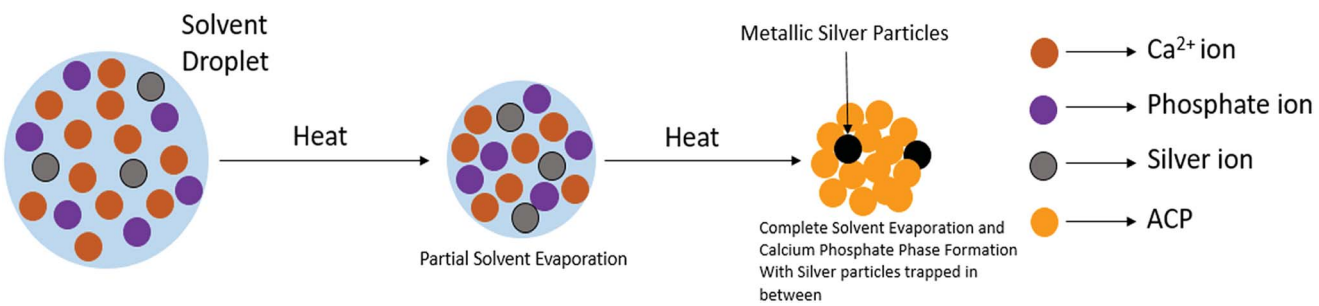

Fig. 2 Pictorial depiction of formation of silver-containing ACP nanoparticles. The solvent droplet initially contains all the ions in solution. As the droplet passes through the heated tube, solvent evaporates, after which calcium and phosphate ions react and precipitate to form the ACP phase, with silver nanoparticles becoming trapped within that phase.

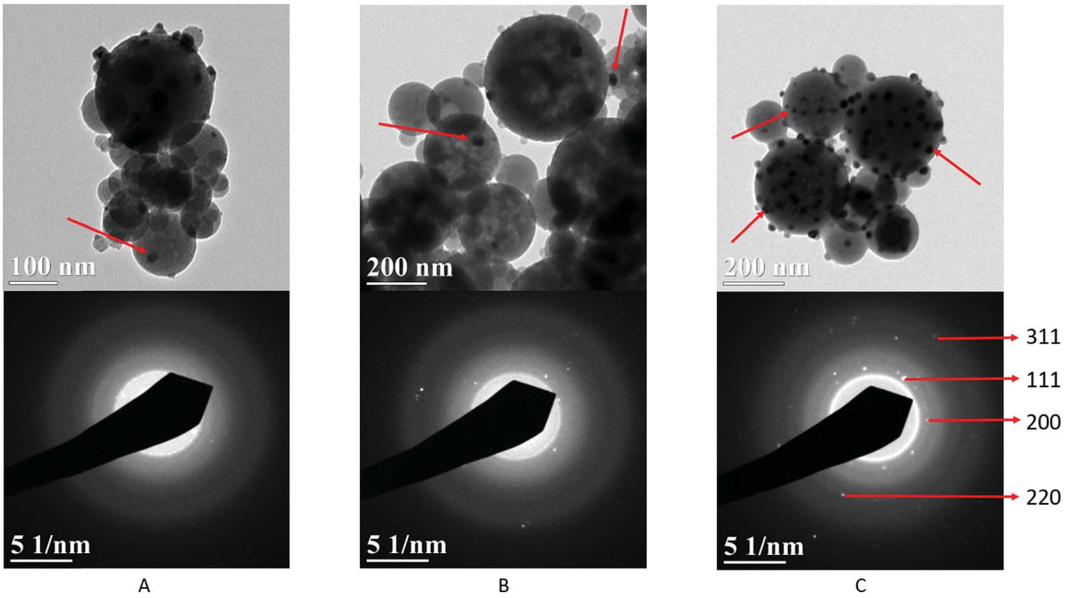

Fig. 3 TEM images of the synthesized particles. (A) Silver-doped ACP particles prepared with 5 mol% silver (relative to calcium) in the precursor solution. The red arrow shows a silver nanoparticle embedded within the ACP phase. The bottom image shows the SAED pattern corresponding to the TEM image, which confirms that the particles are mainly amorphous. (B) Particles with 10 mol% silver. Red arrows show comparatively more silver nanoparticles and the SAED image (bottom) confirms some presence of crystalline silver in the material. (C) Particles with 15 mol% Ag. Silver nanoparticles can be seen embedded within, as well as on the surface, of the ACP particles (indicated by red arrows). The SAED pattern below clearly shows reflections from silver 111, 200, 220, and 311 lattice planes as labelled.

Fig. 3 shows TEM images of the silver-doped ACP nanoparticles with silver clearly seen as the smaller black particles. The SAED image (5 mol% silver) does not show any diffraction pattern, which provides some support for silver particles being very small and dispersed within the ACP particles. However, as the mole percent of silver was increased in the precursor (10% and 15%), there was some indication of a diffraction pattern in SAED images, reflecting both the larger size of silver crystallites present in the sample and higher overall silver concentration. For samples with 10 mol% and 15 mol% silver, shown in Fig. 3B and C, some silver nanoparticles are seen on the surface of ACP particles. SEM imaging (Fig. 4) and elemental mapping by EDS (Fig. 5) clearly show the uniform distribution of the elements and the lack of silver nanoparticles on the surface in the case of 5 mol% silver, with increasing silver nanoparticles on the surface (Fig. 6A and B) as the mole percent is increased to 10% and 15%. EDS detects silver in the synthesized powder, which confirms the presence of silver in the 5 mol% silver sample, even though no silver particles are visible in the SEM images. The EDS signal for silver increases as expected for 10 mol% and 15 mol% samples (Fig. S4, S5 and Table S1†). However, the detected percentage by EDS cannot be considered as the exact percentage in the synthesized material.

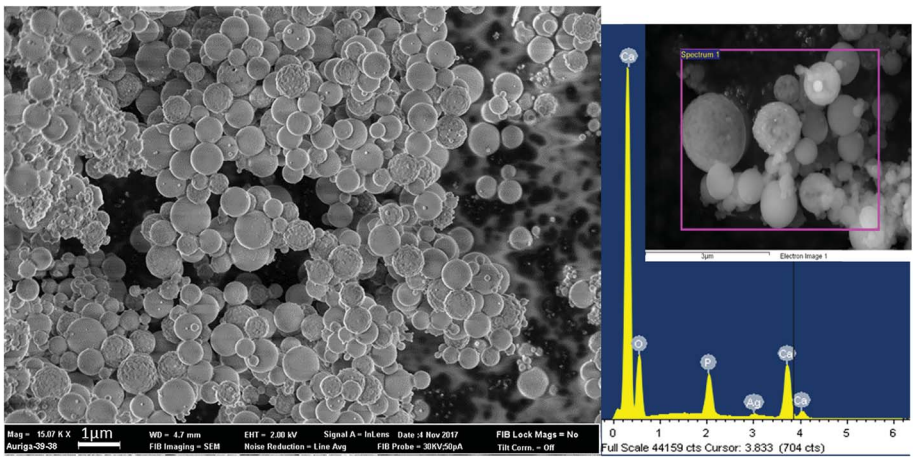

Fig. 4 SEM image of nanocomposite particles with ~5 mol% silver content. There is almost no evidence of silver particles present on the surface of the ACP particles. The EDS spectrum does give some evidence of presence of silver, which can be due to the embedded particles. Inset: image of the region for which the EDS spectrum was acquired.

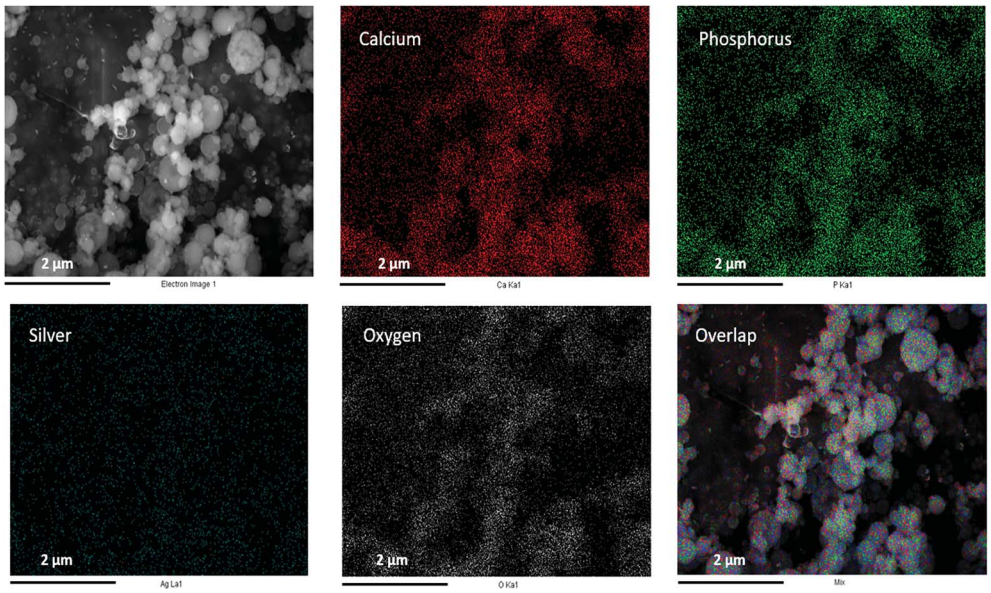

Fig. 5 SEM image (top left) and corresponding EDS-based elemental mapping of ACP particles with 5 mol% silver content.

To further confirm the presence of silver inside ACP particles, XRD was performed on the synthesized material as shown in Fig. 7. First, the XRD pattern without defined peaks corresponds to an amorphous material and shows no crystalline calcium phosphate phases formed. In combination with the elemental composition, this demonstrates success in synthesis of ACP. Second, there was no discernible silver peak in the case of 5 mol% silver. The XRD pattern showed a slight presence of the silver (111) peak in the 10 mol% silver sample, and increased peaks in the 15 mol% silver sample, consistent with

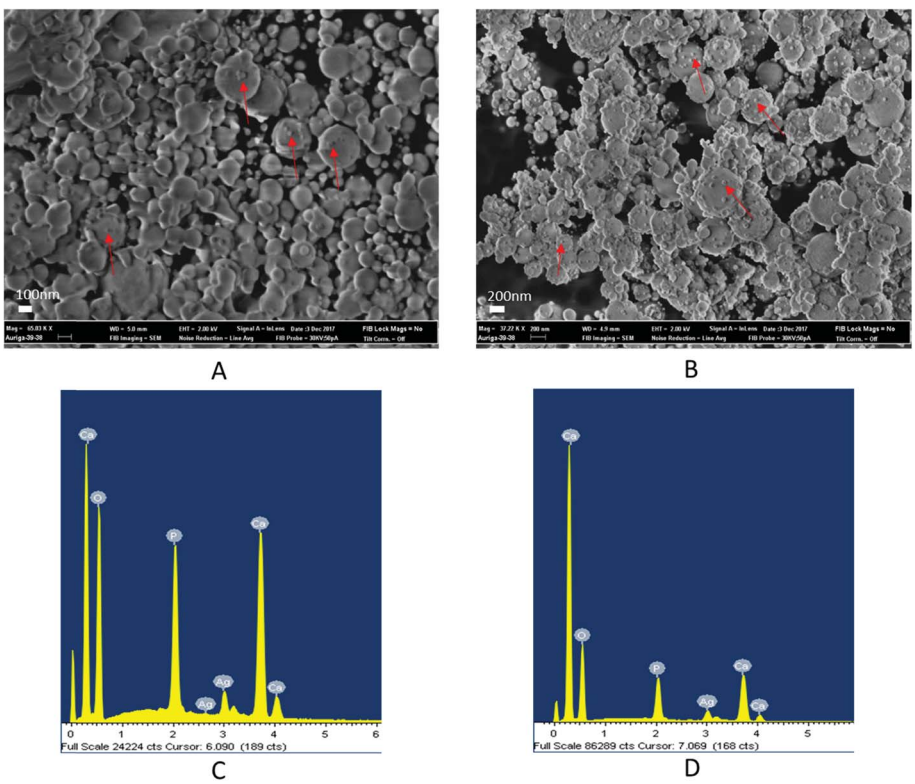

Fig. 6 SEM images for 10 mol% (A) and 15 mol% (B) silver containing ACP samples. The red arrows in (A) and (B) indicate the presence of silver nanoparticles on the surface of the ACP particles. Many more silver nanoparticles are visible on the surface for the 15 mol% silver containing sample compared to 10 mol% and 5 mol% silver. The bottom figures show the EDS spectra for the 10 mol% silver sample (C) and the 15 mol% silver sample (D).

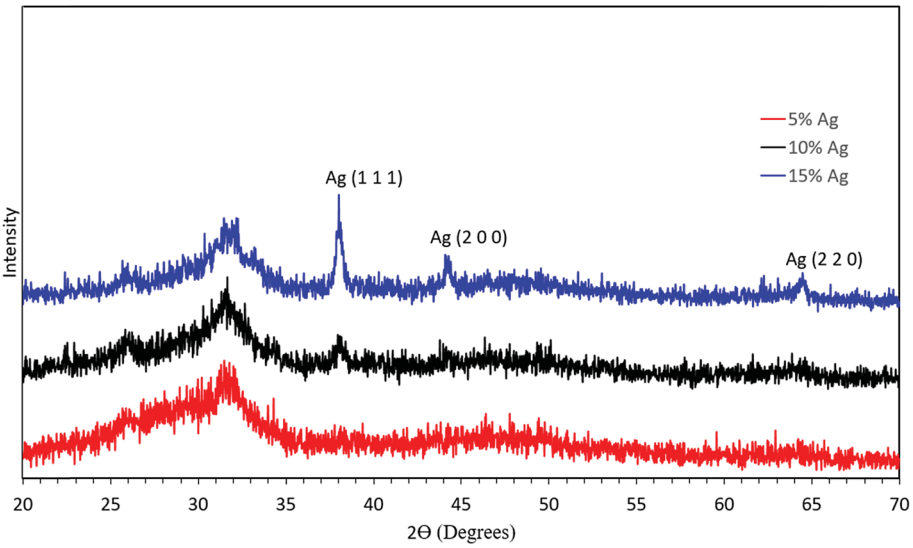

Fig. 7 XRD analysis of the synthesized material with 5 mol% silver (red), 10 mol% silver (black), and 15 mol% silver (blue).

the higher silver content and larger silver crystallites in these samples. If the temperature in the reactor was increased, crystalline calcium phosphate was observed in the product particles (Fig. S1†). Therefore, the temperature set point was kept at 550 °C for further experiments.

ACP particles often must be stored at low temperature to hinder crystallization. Thus, to test the stability of the amorphous material, the synthesized material was exposed to air at ambient temperature (20–25 °C) for a month. The silver–ACP particles showed no crystalline calcium phosphate formation even after 1 month of ambient air exposure as shown in Fig. S2.†

FTIR analysis of the synthesized material (Fig. 8) supported the formation of amorphous calcium phosphate with phosphate bond vibrations seen at 950 cm^{-1} (ν_1 PO_4^{2-}), 600 cm^{-1} (ν_2 PO_4^{2-}) and 1011 cm^{-1} (ν_3 PO_4^{2-}). The broad peak from 2800 cm^{-1} to 3700 cm^{-1} arises from OH bonds due to the presence of water in interstitial spaces of ACP. The peaks at 1340 cm^{-1} and 1420 cm^{-1} which are nitro bond vibrations, may be due to adsorbed NO_2 generated by decomposition of the nitrate precursors. There are no changes observed in the FTIR spectra due to the changing concentrations of silver in the precursor solution (Fig. S3†), which suggests there is no bond formation of any element or group with metallic silver.

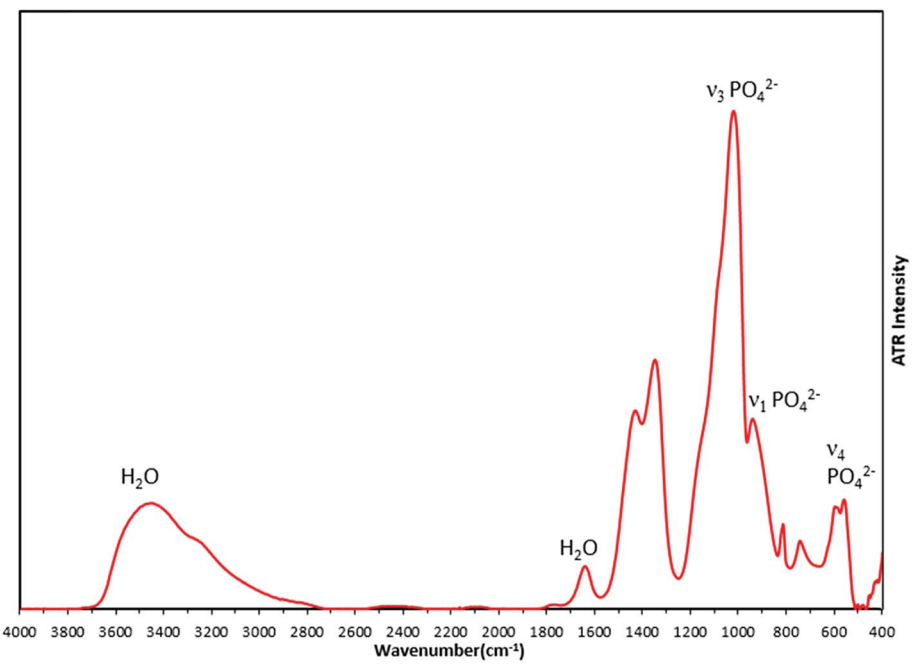

Fig. 8 FTIR spectrum of the synthesized particles (5 mol% silver).

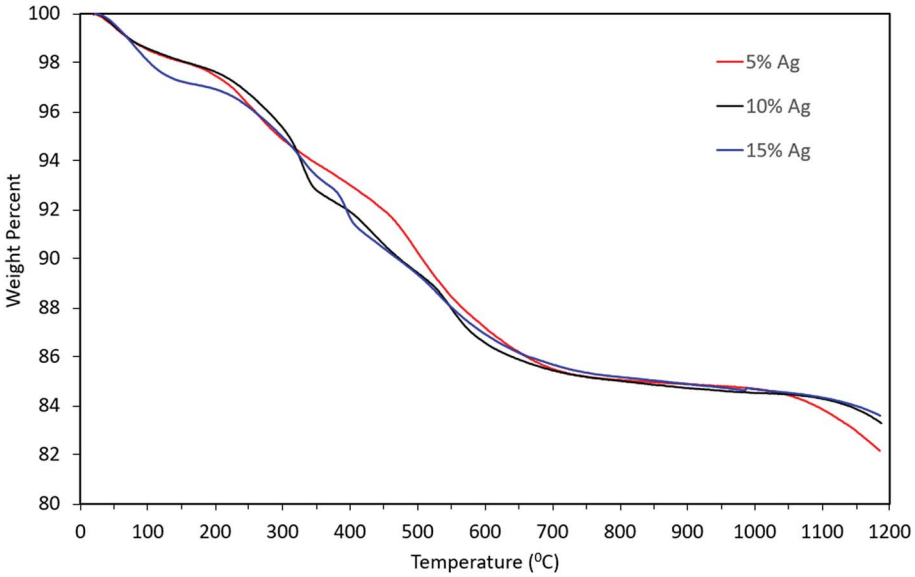

Fig. 9 TGA profiles of the synthesized particles with 5 mol% silver (red), 10 mol% silver (black) and 15 mol% silver (blue). TGA was carried out under nitrogen gas at a flow rate of 100 sccm from room temperature to 1200 °C.

Thermogravimetric analysis of the material indicated that there might be water molecules present, some of which might be adsorbed water *i.e.* the weight loss from 100 wt% to ~97 wt% and remaining weight loss might be due to the presence of tightly bound water molecules (from 97 wt% to 86 wt%). However, the weight loss pattern remained qualitatively similar even as the concentration of silver in the precursor increased, as can be seen from Fig. 9. The overall mass loss was almost identical for the three cases. Slight differences in the TGA curves can be attributed to differences in the rate of desorption and out-diffusion of water at the particular heating rate used (20 °C min^{-1}), due to the presence of silver nanoparticles.

3.2. Release of ions from silver–ACP containing dental adhesive

Discs of silver–ACP nanoparticle-loaded dental adhesive were created as described in the Experimental section, and the

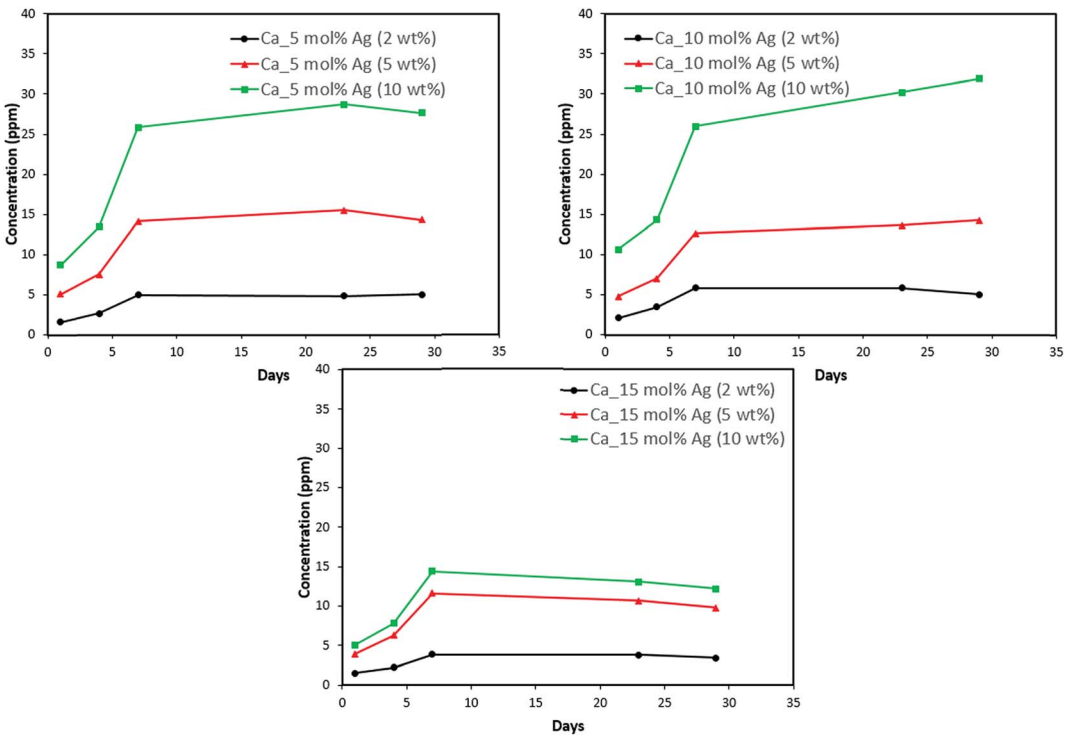

Fig. 10 Calcium release from adhesive resin disc specimens containing 5, 10 and 15 mol% silver with different weight fractions of silver–ACP.

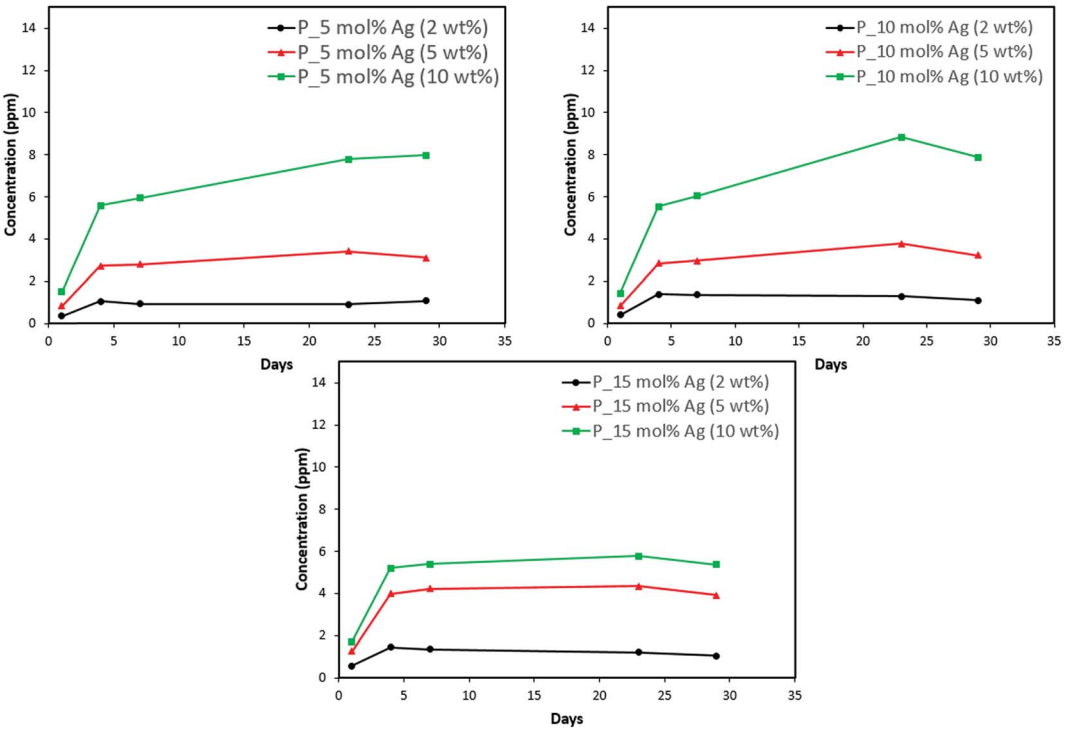

Fig. 11 Phosphorus release from adhesive resin disc specimens containing 5, 10 and 15 mol% silver with different weight fractions of silver–ACP.

release of ions from them under simulated cariogenic conditions was monitored over a period of one month. The objective of this release study was to ascertain whether the silver embedded within ACP particles would provide sustained release of ions. Fig. 10, 11, and 12 present the measured concentrations of calcium, phosphorus, and silver, respectively, detected in the cariogenic solution as a function of time. The small fluctuations in the data points in the above graphs can be attributed to

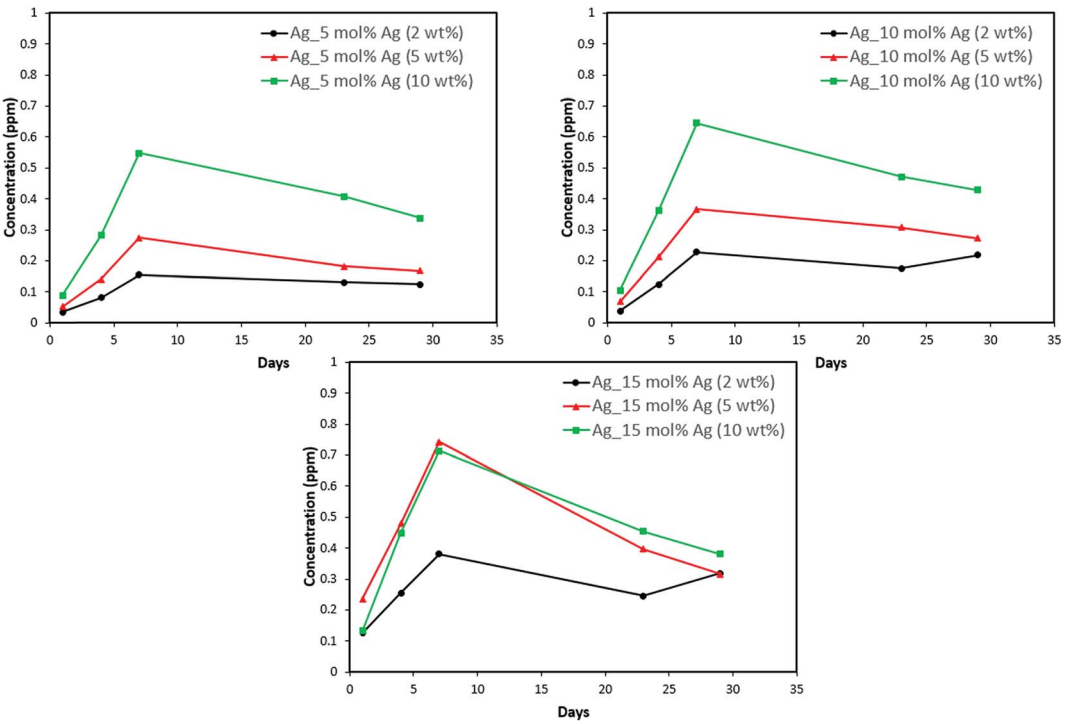

Fig. 12 Silver release from adhesive resin disc specimens containing 5, 10 and 15 mol% silver with different weight fractions of silver–ACP.

fluctuations in the output power of the plasma torch of the ICP. Furthermore, some of the discs with higher weight percent of the silver–ACP material fractured into multiple pieces during the processes of retrieval from the mold, providing additional surface area that was exposed to the simulated cariogenic solution. Despite these factors, the overall trends in release are clear.

The positive results that could be seen from this data are the initial release of calcium, phosphorus and silver in the first few days followed by the sustained presence of ions, which is indicated by the plateau in the graph. However, the gradual loss in concentration of silver could be attributed to the fact that silver ions in water tend to oxidize in the presence of light; and all the solutions were kept under normal room-light conditions. In the case where the silver release is seen again after decrease; the reason could be because of the initial release of silver ions from the particles on the surface of the silver–ACP particle and delayed release occurred as silver embedded inside was exposed to the solution afterwards. Overall, the ion release seems appropriate considering the low weight percentages of silver–ACP.

4. Conclusions

Silver embedded amorphous calcium phosphate particles were synthesized using a spray pyrolysis reactor. To the best of our knowledge, such nanostructures have not been reported before. Silver embedded within the ACP phase may provide better sustained long-term anti-bacterial results than other combinations of these materials. The samples containing 5 mol% silver were found to contain the majority of their silver content dispersed within the ACP particles, whereas the 10 mol% and 15 mol% silver samples had more silver particles on the surface of the ACP particles. The addition of 5 mol% silver containing ACP particles into a commercial dental adhesive at either 2 wt% or 5 wt% loading yielded steady release of the component ions. The 15 mol% silver nanomaterial could be used in cases where there is an immediate requirement for release of more anti-bacterial material, followed by long-term sustained release. Within the limitations of our study, we conclude that the appropriate dispersability and ion release of these nanostructures could have great potential for use as an additive to dental materials.

Conflicts of interest

There are no conflicts to declare.

Acknowledgements

This research was supported by Innovative Micro-Programs Accelerating Collaboration in Themes (IMPACT) from University at Buffalo.

References

1 L. N. Niu, W. Zhang, D. H. Pashley, L. Breschi, J. Mao, J. H. Chen and F. R. Tay, *Dent. Mater.*, 2014, **30**, 77–96.
2 M. A. Melo, S. F. Guedes, H. H. Xu and L. K. Rodrigues, *Trends Biotechnol.*, 2013, **31**, 459–467.
3 L. Zhang, M. D. Weir, L. C. Chow, J. M. Antonucci, J. Chen and H. H. Xu, *Dent. Mater.*, 2016, **32**, 285–293.
4 M. Hannig and C. Hannig, *Nat. Nanotechnol.*, 2010, **5**, 565–569.
5 Y. Ge, B. Ren, X. Zhou, H. H. K. Xu, S. Wang, M. Li, M. D. Weir, M. Feng and L. Cheng, *Materials*, 2017, **10**, 26.
6 H. Colfen, *Nat. Mater.*, 2010, **9**, 960–961.
7 A. Dey, P. H. Bomans, F. A. Muller, J. Will, P. M. Frederik, G. de With and N. A. Sommerdijk, *Nat. Mater.*, 2010, **9**, 1010–1014.
8 H. H. Xu, J. L. Moreau, L. Sun and L. C. Chow, *Dent. Mater.*, 2011, **27**, 762–769.
9 M. A. Melo, S. Orrego, M. D. Weir, H. H. Xu and D. D. Arola, *ACS Appl. Mater. Interfaces*, 2016, **8**, 11779–11787.
10 M. A. Melo, L. Cheng, M. D. Weir, R. C. Hsia, L. K. Rodrigues and H. H. Xu, *J. Biomed. Mater. Res., Part B*, 2013, **101**, 620–629.
11 S. Chen, S. Gururaj, W. Xia and H. Engqvist, *J. Mater. Sci.: Mater. Med.*, 2016, **27**, 172.
12 L. Zhang, M. D. Weir, L. C. Chow, M. A. Reynolds and H. H. Xu, *Sci. Rep.*, 2016, **6**, 36476.
13 L. Cheng, K. Zhang, M. D. Weir, M. A. Melo, X. Zhou and H. H. Xu, *Nanomedicine*, 2015, **10**, 627–641.
14 M. Rai, A. Yadav and A. Gade, *Biotechnol. Adv.*, 2009, **27**, 76–83.
15 K. Lewis, *Antimicrob. Agents Chemother.*, 2001, **45**, 999–1007.
16 J. S. Lee and W. L. Murphy, *Adv. Mater.*, 2013, **25**, 1173–1179.
17 K.-S. Hwang, S. Hwangbo and J.-T. Kim, *J. Nanopart. Res.*, 2008, **10**, 1337–1341.
18 S. V. Dorozhkin, *Acta Biomater.*, 2010, **6**, 4457–4475.
19 C. Combes and C. Rey, *Acta Biomater.*, 2010, **6**, 3362–3378.
20 A. Peetsch, C. Greulich, D. Braun, C. Stroetges, H. Rehage, B. Siebers, M. Koller and M. Epple, *Colloids Surf., B*, 2013, **102**, 724–729.
21 S. Liu, H. Zhang and M. T. Swihart, *Nanotechnology*, 2009, **20**, 235603.